Validation of the estimation of the macrovascular contribution in multi-timepoint arterial spin labeling MRI using a 2-component kinetic model

Plas, M.C.E. van der; Craig, M.; Schmid, S.; Chappell, M.A.; Osch, M.J.P. van

Received: 19 February 2021 | Revised: 19 July 2021 | Accepted: 20 July 2021

DOI: 10.1002/mrm.28960

RESEARCH ARTICLE

Magnetic Resonance in Medicine

Validation of the estimation of the macrovascular contribution in multi-timepoint arterial spin labeling MRI using a 2-component kinetic model

Merlijn C. E. van der Plas[1,2] | **Martin Craig**[3,4,5] | **Sophie Schmid**[1,2] | **Michael A. Chappell**[3,4,5,6] | **Matthias J. P. van Osch**[1,2]

[1]C.J. Gorter Center for High Field MRI, Department of Radiology, Leiden University Medical Center, Leiden, The Netherlands

[2]Leiden Institute of Brain and Cognition (LIBC), Leiden University Medical Center, Leiden, The Netherlands

[3]Radiological Sciences, Division of Clinical Neuroscience, School of Medicine, University of Nottingham, Nottingham, United Kingdom

[4]Sir Peter Mansfield Imaging Center, School of Medicine, University of Nottingham, Nottingham, United Kingdom

[5]Wellcome Centre for Integrative Neuroimaging, Nuffield Department of Clinical Neurosciences, University of Oxford, Oxford, United Kingdom

[6]Nottingham Biomedical Research Centre, Queens Medical Centre, University of Nottingham, Nottingham, United Kingdom

Correspondence
Merlijn C. E. van der Plas, C.J. Gorter Center for High Field MRI, Department of Radiology, C3Q, Leiden University Medical Center, P.O. Box 9600, 2300 RC, Leiden, The Netherlands.
Email: m.c.e.van_der_plas@lumc.nl

Funding information
Engineering and Physical Sciences Research Council UK, Grant/Award Number: EP/P012361/1; Stichting voor de Technische Wetenschappen, Grant/Award Number: 016.160.351

Purpose: In this paper, the ability to quantify cerebral blood flow by arterial spin labeling (ASL) was studied by investigating the separation of the macrovascular and tissue component using a 2-component model. Underlying assumptions of this model, especially the inclusion of dispersion in the analysis, were studied, as well as the temporal resolution of the ASL datasets.

Methods: Four different datasets were acquired: (1) 4D ASL angiography to characterize the macrovascular component and to study dispersion modeling within this component, (2) high temporal resolution ASL data to investigate the separation of the 2 components and the effect of dispersion modelling on this separation, (3) low temporal resolution ASL dataset to study the effect of the temporal resolution on the separation of the 2 components, and (4) low temporal resolution ASL data with vascular crushing.

Results: The model that included a gamma dispersion kernel had the best fit to the 4D ASL angiography. For the high temporal resolution ASL dataset, inclusion of the gamma dispersion kernel led to more signal included in the arterial blood volume map, which resulted in decreased cerebral blood flow values. The arterial blood volume and cerebral blood flow maps showed overall higher arterial blood volume values and lower cerebral blood flow values for the high temporal resolution dataset compared to the low temporal resolution dataset.

Conclusion: Inclusion of a gamma dispersion kernel resulted in better fitting of the model to the data. The separation of the macrovascular and tissue component is affected by the inclusion of a gamma dispersion kernel and the temporal resolution of the ASL dataset.

KEYWORDS
arterial blood volume, arterial spin labeling, cerebral blood flow, dispersion modeling, 2-component kinetic model

1 | INTRODUCTION

Arterial spin labeling (ASL) is a noninvasive MRI technique that allows for the measurement of tissue perfusion. Quantitative cerebral blood flow (CBF) information is important, for example, for studying the hemodynamic involvement in neurovascular diseases such as stroke, Alzheimer disease, and transient ischemic attack.[1,2] For the recommended ASL method of pseudo-continuous ASL (pCASL), the arterial blood is magnetically labeled when traversing through a labeling plane; after a post-label–delay (PLD), in which the labeled blood flows from the labeling plane to the tissue, the readout is performed. Subtracting this labeled image from a control image without magnetic labeling results in perfusion-weighted images. Using a single component model, these perfusion images can be quantified to obtain quantitative CBF maps providing information on the cerebral hemodynamic status of a patient. The main assumption of a single component model is that all labeled blood has arrived at the tissue that it will ultimately supply.

When quantifying the perfusion using a single component model, CBF maps can be contaminated by ASL-signal from within the macrovasculature, that is, label that is still on its way to reach the tissue it will feed, leading to an overestimation of the CBF.[3] Including a macrovascular component into the kinetic model potentially allows for isolation and subsequent elimination of this macrovascular component. This alleviates the overestimation of the CBF because it separates the ASL signal into 2 components: a macrovascular and a tissue contribution. Use of a 2-component kinetic model relies on the availability of multi-time point data and allows generation of both CBF and arterial blood volume (aBV) as well as arterial transit time (ATT) maps. However, only limited validation of this 2-component model has been performed.[3,4]

Due to underlying assumptions of the 2-component model, the CBF maps can still be biased. For example, it is frequently assumed that the box-shaped input function as it is created at the labeling plane is preserved when it travels through the vasculature into the tissue.[5] However, due to laminar flow profiles in larger arteries, bifurcations, bending of vessels, and diffusion of the labeled water molecules within the blood, the labeled bolus will be dispersed.[6] Therefore, to obtain more realistic CBF estimations, it has been proposed to include a gamma distribution dispersion kernel in the 2-component model to estimate and correct for dispersion of the bolus of labeled blood. By correcting the CBF quantification for the fact that some dispersed (trailing) spins have not yet arrived at their final destination, the perfusion estimation can be improved, and such a correction would lead to higher CBF values.[7,8] On the other hand, it could also potentially improve the discrimination between the macrovascular and tissue perfusion signal, which would lead to higher aBV values and lower CBF values.

Fitting multi-timepoint ASL data with a 2-component kinetic model allows for the estimation of CBF, aBV and ATT maps. Timing parameters such as ATT have proven to provide important information in patients with, for example, transient ischemic attack, Alzheimer disease, and stroke.[1,2,9] Separation of the macrovascular signal from the tissue signal allows for more accurate CBF values because the CBF estimations are no longer contaminated by macrovascular signal.[3] It is, however, difficult to separate the 2 components especially far into the arterial tree because at this point the macrovascular signal is more dispersed and looks very similar to tissue signal. Including a dispersion kernel within this 2-component kinetic model will improve the separation at this point because it can assess macrovascular dispersion.[6] Therefore, accuracy of the CBF estimation could potentially be improved by fitting multi-timepoint ASL data with a 2-component kinetic model with dispersion modelling.

The goal of this study was to validate the separation of the macrovascular and tissue component by the 2-component model and to validate the underlying assumptions with a special focus on the inclusion of dispersion in the analysis. This was studied by acquiring both 4D ASL angiography (ASL-MRA) to better characterize the vascular component, as well as high and low temporal resolution ASL-data to test whether temporal resolution affects the ability to estimate the macrovascular component. In this study, the term *temporal resolution* stands for the temporal sampling interval with which the passage of label was imaged; for traditional ASL, this would be equal to the PLD step-size.

2 | METHODS

2.1 | MRI experiments

Eight healthy volunteers (22-56 years old; 7 females, 1 male) were scanned using a 32-channel head coil on a 3 Tesla-scanner (Achieva, Philips Healthcare, Best, The Netherlands). All volunteers provided informed consent, and the study was approved by the local institutional review board. In each volunteer, 4 datasets were acquired: (1) 4D ASL angiography for detailed information on the macrovascular signal; (2)

high temporal resolution perfusion ASL data; (3) conventional (low) temporal resolution perfusion ASL data; and (4) conventional (low) temporal resolution perfusion ASL data with vascular crushers.

2.2 | Characterization of the macrovascular component and dispersion using 4D ASL-MRA

2.2.1 | Acquisition

As a reference scan for the macrovascular component, 4D contrast inherent inflow-enhanced multiphase angiography ASL data was acquired.[10] pCASL labeling with a label duration of 500 ms was followed by a minimum PLD of 40 ms and a Look-Locker (LL) turbo-field echo-planar imaging readout, by which 8 images were acquired at an interval of 200 ms with a constant flip angle of 7°.[11,12] In total, 140 slices were acquired in 6 min 44 s (TR/TE = 12/4.7 ms; multi-shot 3D turbo-field echo-planar imaging with 91 shots, and EPI factor of 5) with a FOV of 220×220 mm^2, an acquisition voxel size of $1.27 \times 1.27 \times 1.30$ mm^3, and a sensitivity encoding factor of 2.5 (Figure 1A). For calibration purposes, an M0 image with the same geometry and parameters was acquired without employing LL and using a flip-angle of 10°. Note that instead of the more commonly used pulsed labeling scheme, a pCASL labeling approach was used for this 4D ASL angiography dataset to keep the acquisition as similar to the perfusion data as possible.

2.2.2 | Postprocessing

The 4D angiography data was corrected for the use of a low flip-angle LL readout by calculating the amount of saturation[12]:

$$M_z(t+1) = M_z(t) \cdot \cos\left(\alpha_1\right) \cdot \cos\left(\alpha_2\right) \cdot \cos\left(\alpha_3\right) \cdot \cos^n(\alpha)$$

$$M_{xy}(t) = M_z(t) \cdot \sin(\alpha),$$

where α_1, α_2, and α_3 are the flip angles of the startup echoes; α is the flip angle of 7° that was used during the acquisition; and n is the amount of RF pulses that were used during a single LL phase. After subtracting the label condition from the control condition, the 4D ASL angiography was divided by the appropriate correction factor as calculated for that LL phase.

The corresponding M0 scan that was used to quantify this dataset was scanned with a different flip angle ($\alpha = 10°$) and a shorter TR of 800 ms. To correct for this, the longitudinal magnetization was modelled as follows[13]:

$$M_z(t) = M_z(t-1) * e^{-\frac{TR}{T1,b}} + \left(1 - e^{-\frac{TR}{T1,b}}\right)$$

$$M_z(t) = M_z(t) * \cos(\alpha).$$

The longitudinal magnetization was calculated over the multiple RF pulses that were used during the readout, showing that it reached a steady state at 0.66. Multiplying by $\sin(\alpha)$ to account for the low flip-angle excitation provided the correction factor. The M0 scan was divided by this correction factor before quantifying the data with a kinetic model (see next section). A single M0 value calibration technique was used during quantification because the M0 scan was inhomogeneous due to fresh inflow of blood within the vasculature.[14]

2.2.3 | Kinetic modeling

The Bayesian Inference for Arterial Spin Labeling MRI (BASIL) toolkit of the Oxford Centre for Functional MRI of the BRAIN's software library was used to quantify the ASL signal within a probabilistic analysis approach.[3,15,16] Within this framework, the macrovascular contribution to the ASL signal can be fitted and separated from the perfusion signal using the 2-component kinetic model. This results in CBF, aBV, and ATT maps. The negative free energy (FE) was calculated, which combines the accuracy of the fit of the model with a penalty for the number of free parameters; the higher this value, that is, the closer to 0 because the values are negative, the better the model was able to fit the data. In addition, the model's fit prediction was obtained showing how the model fitted the data over the multiple timepoints. A single M0 value, which was determined manually in a region of interest located in the gray matter and divided by the tissue/blood partition coefficient of water ($\lambda = 0.9$), was used for calibration.

For this 4D ASL angiography dataset, only the macrovascular component was fitted, resulting in only aBV maps, that is, no CBF and ATT maps. Moreover, fitting was restricted to the first 5 timepoints of the data because barely any signal was present in the last 3 timepoints. Three different models were tested: (1) without dispersion, that is, assuming a boxcar-shaped bolus shape; (2) with inclusion of dispersion by a gamma kernel using the default settings of BASIL for the parameters time to peak (p) and sharpness (s) (parameters reparametrized and subject to a Gaussian prior with means and precisions; default values for the priors of these parameters described by $\log(s) = 2$ and $\log(s*p) = -0.3$, with the precision of these priors set at 1.0); and (3) with inclusion of a gamma dispersion kernel with low precision priors. For this model, more freedom to the dispersion kernel was achieved by lowering the precisions of the priors from 1.0 to 0.1 for the 2 parameters (p and s) that are described earlier .

The default value for the prior of the parameter that describes the time it takes for the bolus to arrive within an

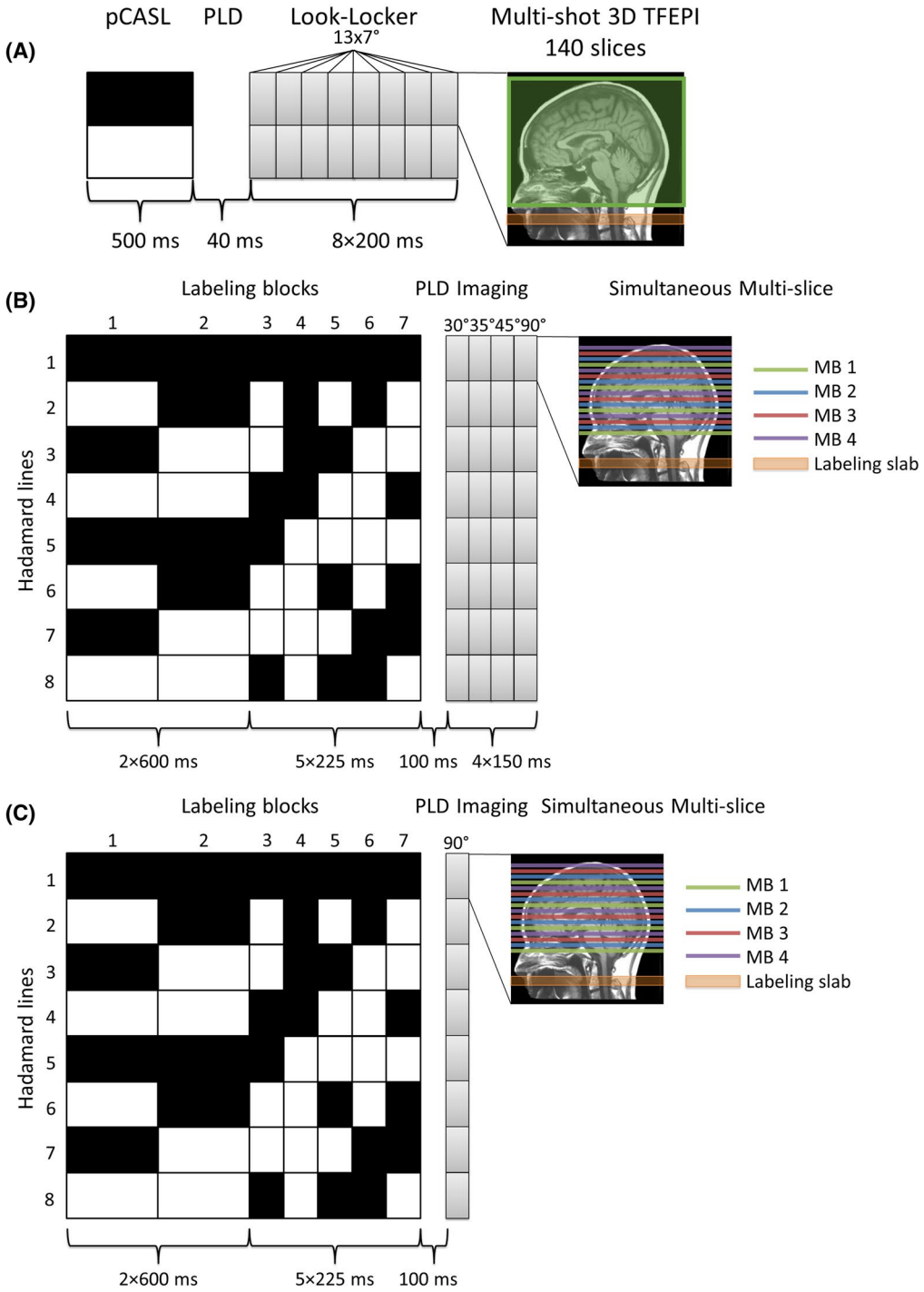

FIGURE 1 (A) Overview of the sequence used to acquire the 4D contrast inherent inflow-enhanced multiphase angiography ASL angiography. A pCASL labeling with a duration of 500 ms was followed by a low flip-angle LL multi-shot 3D TFEPI readout that acquired 8 images at an interval of 200 ms. (B) Overview of the high temporal resolution sequence based on a Hadamard-8 labeling scheme for time-encoded pCASL in combination with a LL readout. The total label duration of 2325 ms was divided into 7 blocks of 2 × 600 ms and 5 × 225 ms, with a minimum PLD of 100 ms. The black blocks indicate labeling; the white blocks indicate control condition; and the numbers below the blocks represent the duration in milliseconds. Background suppression pulses were played out at 1060 and 2020 ms after start of labeling. By means of the LL readout, 4 phases of 150 ms were acquired with each a different flip angle: 30°, 35°, 45° and 90°. Four slices were excited simultaneously by using a simultaneous multi-slice acquisition. (C) Overview of the low temporal resolution sequence based on a Hadamard-8 labeling scheme. By eliminating the LL readout for this sequence, 7 timepoints were acquired using a 90° flip angle. This sequence was performed with and without vascular crushing of 4 cm/s^2. ASL, arterial spin labeling; LL, Look-Locker; MB, multiband; pCASL, pseudo-continuous ASL; PLD, post-label delay; TFEPI, turbo-field echo-planar imaging

arterial voxel also described as bolus arrival time (BAT), which is set in BASIL to 1 s as default value for pCASL, is based on different acquisition settings than those used for this study. For the 4D ASL angiography, a shorter value was observed for BAT because a short label duration and PLD were used. However, because no prior experience was available, the first 4 datasets were used to explore multiple different initialization values for the prior of the BAT parameter ranging from 0.1 to 1 s with steps of 0.15 s, and subsequently the parameter was fixed.

To determine which model was able to best estimate the macrovascular component, the mean negative FE was calculated within an arterial mask, and the model's fit predictions were investigated. The arterial mask was created manually by thresholding the aBV maps for the 3 different models for each volunteer. Only the voxels that were included in all 3 masks were included in the arterial mask that was used for the evaluations. The mean negative FE was also used to determine which of the initialization values for the BAT parameter provided the best fit to the data in the preliminary experiments to set the BAT prior mean value. The mean aBV values were also calculated within the arterial mask. A univariate analysis of variance (ANOVA), with $P < .05$ to be considered significant, was used to compare the mean aBV values between the 3 models that were fitted to the data.

2.3 | Combined estimation of dispersion and macrovascular component in high temporal resolution ASL

2.3.1 | Acquisition

To study the ability to estimate dispersion and to separate the macrovascular component from the tissue component, high temporal resolution ASL datasets were acquired. Densely sampled multi-timepoint (28 timepoints) ASL was acquired by combining time-encoding pCASL with a Hadamard-8 matrix and a LL EPI readout (Figure 1B).[17] The total label duration for the time-encoding-pCASL was 2325 ms, which was divided into 7 blocks of 2 × 600 ms and 5 × 225 ms, with a minimum PLD of 100 ms. Two frequency offset corrected inversion pulses were applied at 1060 and 2020 ms for background suppression. By employing a LL EPI readout in combination with a flip-angle sweep of 30°, 35°, 45° and 90°, 4 images were acquired at an interval of 150 ms while maintaining an approximately constant signal over the multiple LL readouts. To obtain whole brain coverage, that is, 16 slices, within the 150 ms interval, 4 slices were excited simultaneously with multi-banded RF pulses. For these 16 slices, a total of 12 repeats of the 8 Hadamard encoded images (96 acquisitions) were acquired in 10 min 20 s (TR/TE = 3100/9.52 ms; fat suppression by means of spectral presaturation with inversion recovery; single-shot echo planar imaging), with a FOV of 220 × 220 mm^2 and a voxel size of 3 × 3 × 8 mm^3. A sensitivity encoding factor of 1.9 was used in combination with a partial Fourier imaging factor of 0.7.[18] For calibration purposes, an M0 image with the same geometry, flip-angle of 90°, and a TR of 2000 ms was acquired without utilizing LL or simultaneous multi-slice acquisition.

2.3.2 | Postprocessing

The high temporal resolution ASL dataset was decoded using the appropriate Hadamard matrix. The following three corrections were performed before quantifying the ASL signal, background suppression correction, correction for the loss of signal due to imperfect inversion and a correction for the use of the flip-angle sweep.[18]

2.3.3 | Kinetic modeling

Both the macrovascular and perfusion components were modeled for the high temporal resolution ASL dataset, thereby producing CBF, aBV, and ATT maps. A single M0 value calibration method was used, which was manually determined using a region of interest in the gray matter and corrected for $\lambda = 0.9$. Two different models were fitted to the high temporal resolution dataset: (1) without dispersion modelling, and (2) with a gamma dispersion kernel included in the model. Fitting the data with these 2 models will provide insight on how the model is able to estimate both the macrovascular component and the dispersion within a 2-component kinetic model. The initialization value for the BAT parameter that gave the highest mean negative FE for the 4D ASL angiography was used.

To calculate the mean aBV and CBF values for this dataset, gray matter masks were created by segmenting a T_1-weighted image using FMRIB's automated segmentation tool in FSL, which was followed by a registration to ASL space. Arterial masks were obtained by manually thresholding averaged ASL images for the second through ninth timepoints. A multivariate ANOVA was used to compare the mean aBV and CBF values between the 2 models, where $P < .05$ was considered as significant.

The mean aBV values were subsequently compared with the mean aBV values obtained from the 4D ASL angiography. Because the reconstructed spatial resolution of the high temporal resolution dataset (2.625 × 2.625 × 8 mm^3) differs from the reconstructed spatial resolution of the 4D ASL angiography dataset (0.86 × 0.86 × 0.65 mm^3), the 4D ASL angiography was down-sampled using an averaging filter of 3 × 3 × 12 voxels in MatLab R2019b (MathWorks, Natick, MA) before quantification to achieve similar spatial

resolution. For this downsampled 4D ASL angiography, only the macrovascular component was fitted, and only to the first 5 timepoints — as with the original 4D ASL angiography dataset because barely any signal is left during the last 3 phases.

2.4 | Effect of temporal resolution on separation of macrovascular and tissue component in multi-timepoint ASL

2.4.1 | Acquisition

To study the effect of the temporal resolution of an ASL dataset on the separation of the macrovascular and tissue component, a conventional (low) temporal resolution dataset was also acquired by eliminating the LL readout and using a 90° flip-angle for the 2D multi-slice readout (Figure 1C). This results in only 7 timepoints compared to the 28 timepoints of the high temporal resolution dataset. This low temporal resolution data was acquired twice, with and without vascular crushing in the inferosuperior direction, with a velocity encoding cutoff of 4 cm/s^2. All other parameters were kept constant. In addition, a synthetic low temporal resolution ASL dataset was obtained from the high temporal resolution ASL dataset by eliminating the last 3 LL readouts for every Hadamard line. Using this approach, the effect of different acquisitions can be avoided while the influence of the temporal resolution can still be studied.

2.4.2 | Postprocessing and kinetic modeling

Postprocessing of the low temporal resolution data was the same as for the high temporal resolution data, and the same kinetic models were fitted. The synthetic low temporal resolution ASL dataset was corrected for the fact that it was acquired with a 30° flip angle, whereas other postprocessing and analyses was kept equal to the original low temporal resolution ASL dataset. Comparison of the mean aBV and CBF values was performed for the 2 different ASL datasets to investigate whether separation of the 2 components was affected by the temporal resolution of the data. This comparison between different temporal resolutions was statistically tested using a multivariate ANOVA where $P < .05$ was considered as significant.

3 | RESULTS

3.1 | Characterization of the macrovascular component and dispersion using 4D ASL-MRA

Figure 2 shows the 4D ASL angiography from a representative volunteer as maximum intensity projections. Images were acquired at an interval of 200 ms; therefore, the passage of the labeled blood within the arteries can be followed clearly. Because this dataset only contains macrovascular signal, only the macrovascular component of the kinetic model was fitted, resulting in aBV maps, as shown in Figure 3 for

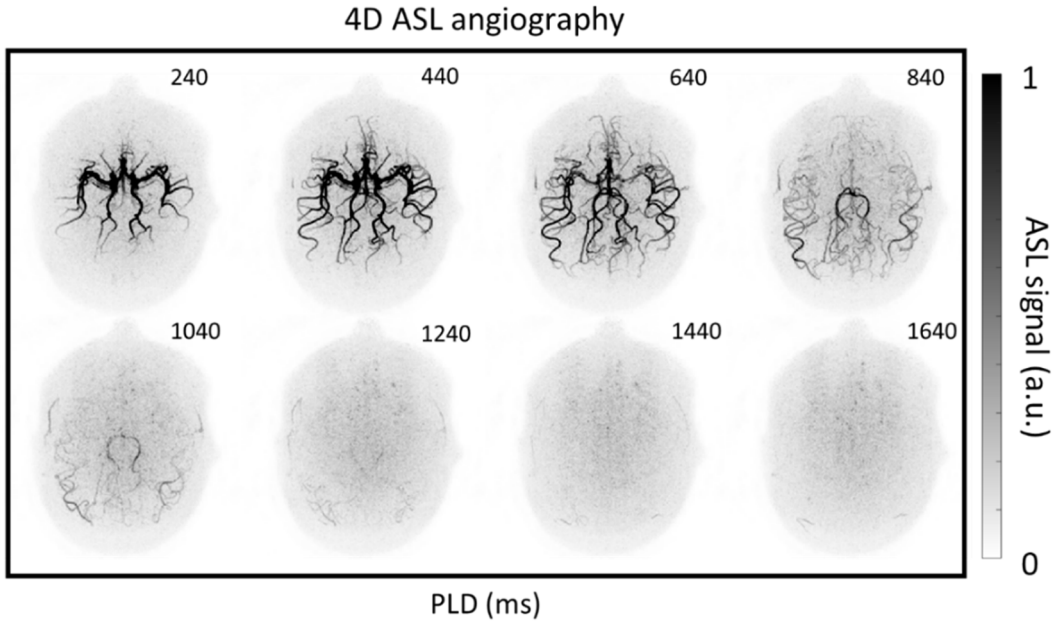

FIGURE 2 Maximum intensity projections for 8 different timepoints of the 4D ASL angiography scan. The PLD ranged from 240 to 1640 ms, which allowed for imaging of the labeled blood traversing the macrovasculature. The pCASL label duration was only 500 ms; thus, the signal intensity was decreased for the last 3 timepoints because the bolus of labeled spins traversed the vasculature

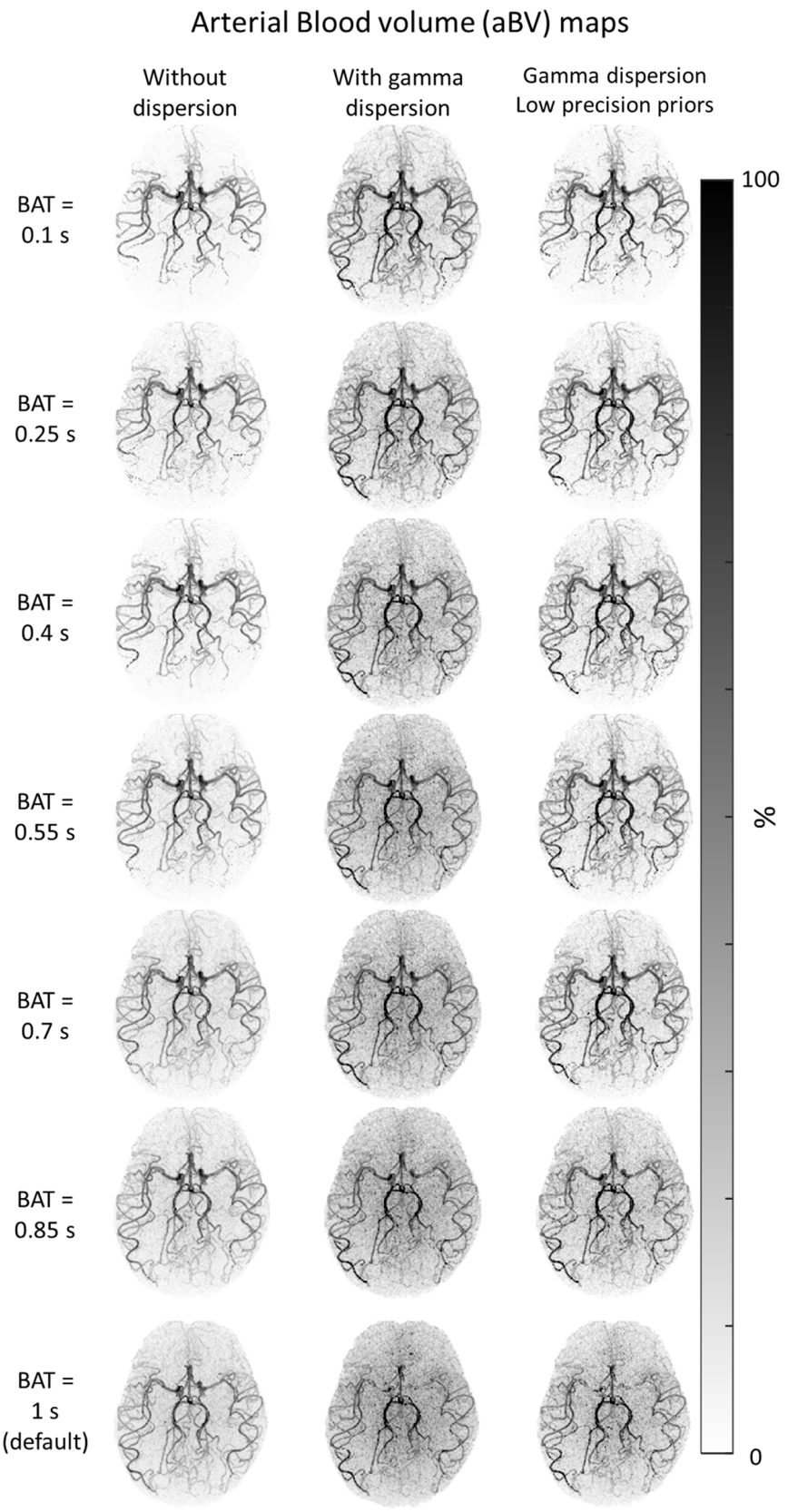

FIGURE 3 ABV maps estimated using different initialization values for the BAT in the arterials for the 3 different models: without a dispersion kernel included, with a gamma dispersion kernel included, and with a gamma dispersion kernel included with low precision priors. The aBV maps for the model without the dispersion included show a dependency on the initialization value, whereas the aBV maps for the model with the gamma dispersion included are less dependent. For all 3 models, without dispersion, with dispersion and with dispersion with lower precision priors, applies that more signal in the background is present using a higher value for the BAT parameter. ABV, arterial blood volume; BAT, bolus arrival time

the 3 tested models, in combination with the different initialization values for the BAT parameter. Especially for the model without inclusion of a dispersion kernel, the signal in the aBV maps is dependent on the BAT initialization value. Increasing, BAT values for this model resulted in an increase of estimated aBV because signal was fitted further down the vascular tree. Increasing BAT values also resulted in higher nonnegligible values outside the macrovasculature, which

could be due to successful fitting of label further upstream in the vascular tree and/or inclusion of tissue signal in the fitted signal. Ideally, higher spatial resolution should be required to pinpoint what these nonnegligible values are representing. At the moment, we would characterize these signals as *tissue blush*, as similarly found in digital subtraction angiography. When a gamma dispersion kernel was included in the model, the aBV maps were more consistent over the different initialization values, and more nonnegligible values outside the macrovasculature were observed. For the default BAT value of 1 s, the model was not able to fit the signal in the middle cerebral artery. This is also the case when applying the model with low precision priors for which the precision on the priors for the 2 dispersion parameters was reduced to give the dispersion kernel more variability when fitted from the data. For this model, more variations in the aBV map are seen for the multiple initialization values. However, a decrease in number of nonnegligible values outside the macrovasculature is shown compared to the model with default settings for the gamma dispersion kernel.

Figure 4A shows example fits for 4 representative voxels in which the different models were fitted to the 4D ASL angiography dataset with a prior value of BAT = 0.55 s. Overall, the model that includes the gamma dispersion kernel showed the best similarities with the ASL signal over time, which is supported by the highest, that is, the closest to 0, mean negative FE values within the macrovascular component (Figure 4B). The model without the inclusion of a gamma dispersion kernel and the model with the gamma dispersion kernel included with low precision priors were both not able to fit the macrovascular ASL signal in all voxels. Subsequently, the mean negative FE was calculated over the arterial mask to determine the best model in combination with the best initialization value for the BAT parameter, which are shown in the graphs in Figure 4B. This analysis was first performed in half of the volunteers as an initialization study. Based on the mean negative FE, the model with the gamma dispersion kernel was selected. This model also showed the most consistent aBV maps over the range of different initialization values for BAT. The BAT initialization was favorable in a range of 0.25 till 0.7 s, that is, showing the highest mean negative FE. We decided to take the approximate middle value for our analysis to be on the safe side and to stay clearly away from the steep decrease of FE values after 0.7 s. Therefore, a BAT value of 0.55 s was used for all further analyses.

To study the effects of modelling dispersion on the detection of the macrovascular component, mean aBV values were calculated within the arterial mask (Table 1). Including a gamma dispersion kernel in the model resulted in an increase of mean aBV values for all volunteers (Figure 3). Lowering the low precision priors of the gamma dispersion kernel lead to a small decrease compared to the aBV map for the default gamma dispersion model. An univariate ANOVA test on the outcome variable, mean aBV values, revealed significant effects between the 3 different models that were fitted to the data ($F(2,21) = 16.229$, $P < .001$).

3.2 | Combined estimation of dispersion and macrovascular component in high temporal resolution ASL

Figure 5A shows a single slice out of the 16 slices that were acquired with high temporal resolution ASL. A temporal resolution of 75 ms was achieved up to a PLD of 1525 ms. The signal fluctuations in intensity of the ASL-images can be explained by the different label durations for the sub-boli of the Hadamard-8 preparation. BASIL accounts and corrects for these differences in the applied model.

A 2-component model was fitted to this multi-timepoint ASL dataset; therefore, aBV and CBF maps were obtained (Figure 6). Mean aBV and CBF values were calculated, which are shown in Table 2. For this dataset, mean aBV values were increased when dispersion was included in the model. In addition, a decrease in CBF values was found, as shown in Figure 6 and Table 2. The multivariate ANOVA test showed a significant difference in CBF and aBV for the 2 models ($F(2, 13) = 52.460$, $P < .001$; Wilks' $\Lambda = 0.110$). Subsequent univariate ANOVAs on the outcome variables revealed significant effects for both CBF ($F(1,14) = 6.632$, $P = .022$) and aBV values ($F(1,14) = 48.733$, $P < .001$).

The first 3 rows of Figure 7 show the aBV maps created with the 3 models for the different datasets (4D ASL angiography, the downsampled 4D ASL angiography, and the high temporal resolution ASL). When comparing the aBV values from the high temporal resolution ASL dataset (1.44%, mean aBV values for all volunteers without dispersion) with the aBV values for the downsampled 4D ASL angiography dataset (15.89%, mean aBV values for all volunteers without dispersion), the aBV values for the multi-timepoint ASL datasets were found to be much lower.

3.3 | Effect of temporal resolution on separation of macrovascular and tissue component in multi-timepoint ASL

Figure 5B shows a single slice out of the 16 slices that were acquired with the lower temporal resolution, both with and without vascular crushing of 4 cm/s^2. Seven time points were acquired with a temporal resolution of 225 ms for the earlier PLDs and 600 ms for the latest PLDs. Inclusion of vascular crushing resulted in a decrease of signal in the earlier timepoints due to saturation of the fast-flowing blood in the macrovasculature.

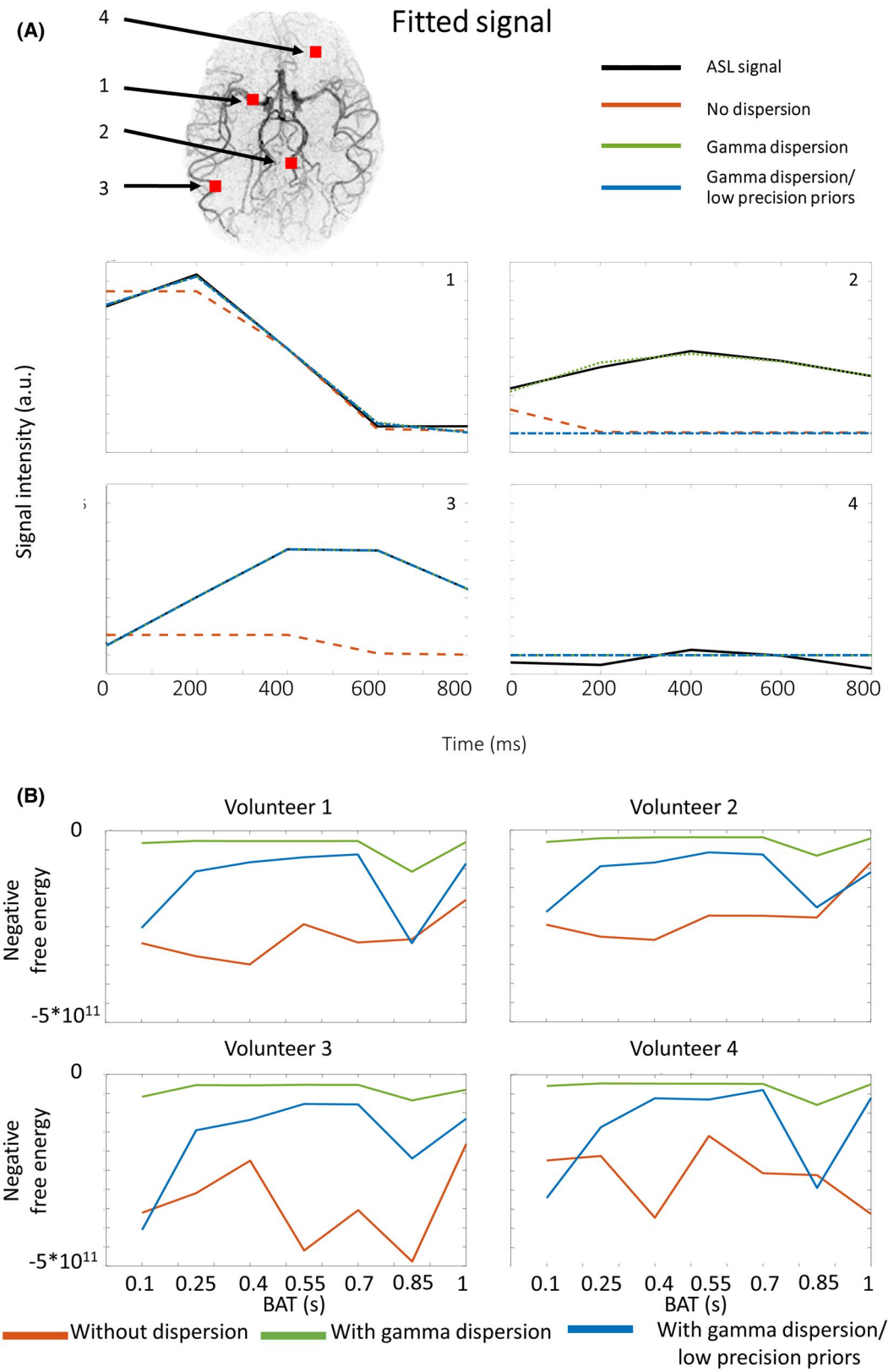

FIGURE 4 (A) Model's fit prediction over the multiple timepoints for the 3 different models that were fitted to the 4D ASL angiography. The black line is the subtracted ASL signal over the multiple timepoints, and the different colors represent the different models all using the initialization value of 0.55 s for the BAT parameter. The model with the inclusion of a gamma dispersion kernel but without the extra freedom was able to fit the subtracted ASL signal over time the best. (B) Mean negative free energy values within an angiographic mask for the multiple volunteers and the different models in combination with a range of initialization values for the BAT parameter. The mean negative free energy values are the highest for the model with the gamma dispersion kernel included. In addition, for this model the negative free energy remains stable over the different initialization values

TABLE 1 Mean aBV values in percentages for 4D ASL angiography

	Without Dispersion	With Gamma Dispersion	With Gamma Dispersion (low precision priors)
Volunteer 1	46.75%	68.74%	65.67%
Volunteer 2	38.10%	69.47%	65.34%
Volunteer 3	46.24%	70.08%	67.10%
Volunteer 4	54.49%	72.67%	71.38%
Volunteer 5	63.24%	78.99%	75.77%
Volunteer 6	53.98%	62.84%	61.20%
Volunteer 7	53.48%	60.90%	60.04%
Volunteer 8	54.03%	61.91%	60.57%
Mean	51.29%*	68.20%*	65.88%*

ANOVA, analysis of variance.

*Statistically different, univariate ANOVA, $P < .05$.

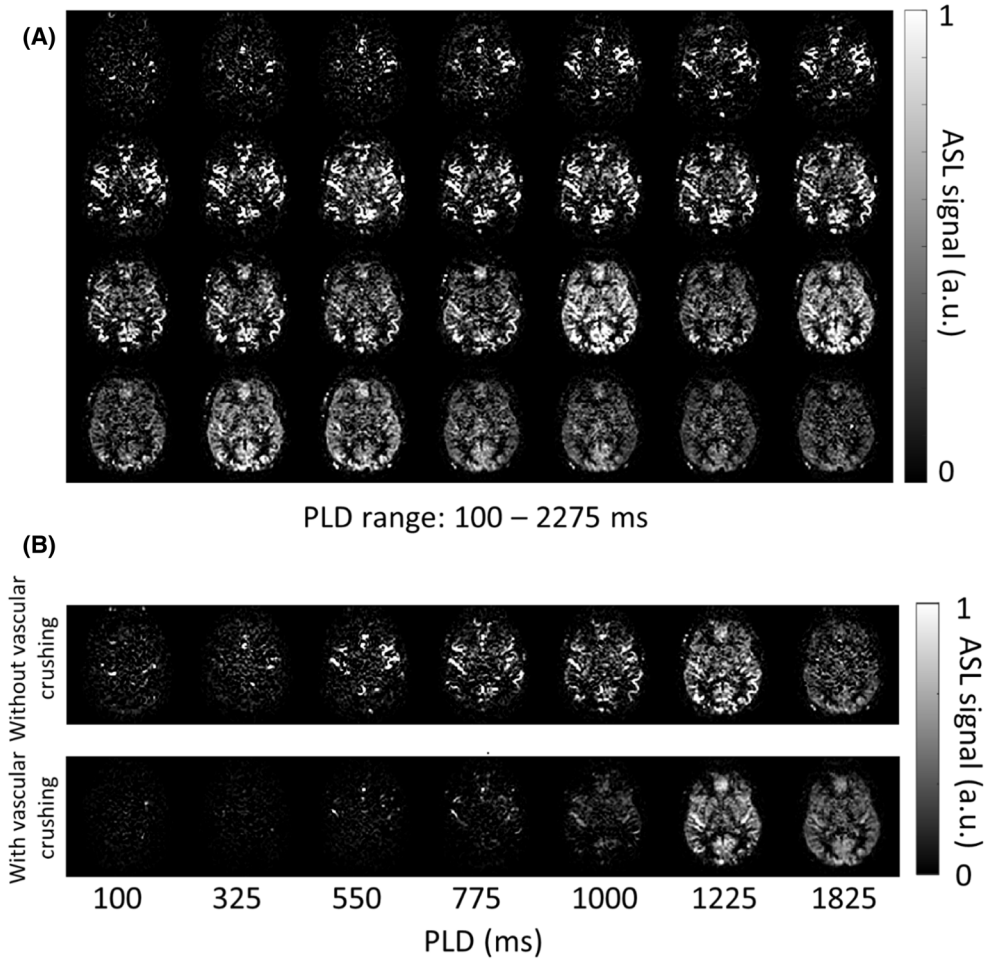

FIGURE 5 (A) Subtracted ASL signal for a representative single slice from the high temporal resolution dataset. Twenty-eight chronological timepoints are shown with a temporal resolution of 75 ms up to a PLD of 1525 ms. B) Subtracted ASL signal for a representative single slice from the low temporal resolution dataset. Seven chronological timepoints are shown without (top) and with (bottom) vascular crushing of 4 cm/s^2. The dataset with the vascular crushing shows almost no signal at the earlier PLDs, proofing that the fast-flowing blood was effectively crushed. a.u. = arbitrary units

Figure 6 shows the aBV and CBF maps for the low temporal resolution ASL dataset, with and without vascular crushing. Mean aBV and CBF values are shown in Table 2. Inclusion of a gamma dispersion kernel resulted in an increase in aBV and a decrease in CBF values. For the dataset with the vascular crushing, almost no signal

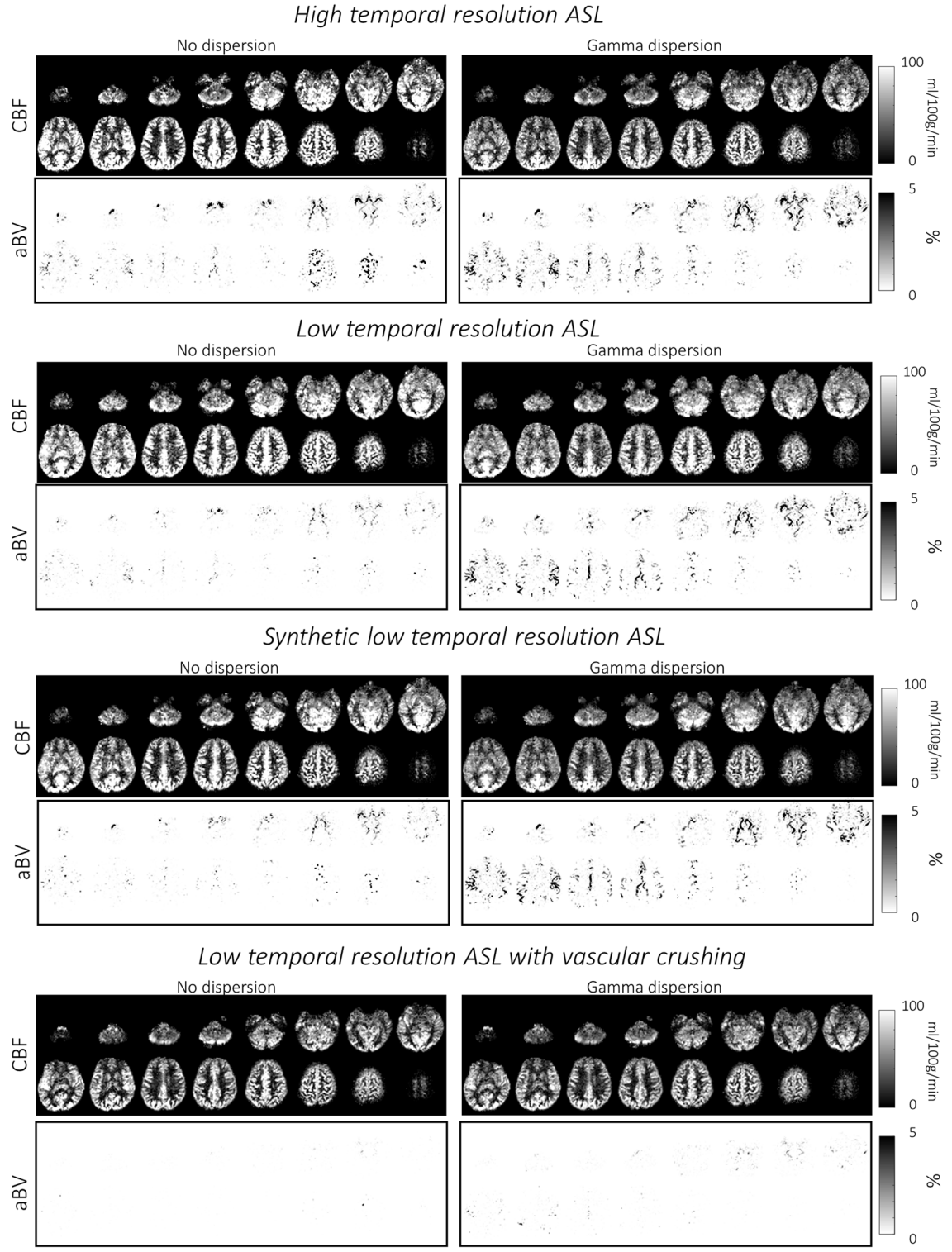

FIGURE 6 aBV and cerebral blood flow (CBF) maps for volunteer 3 for the high and (synthetic) low temporal resolution, and for the latter with vascular crushing. More macrovascular signal is included in the aBV map for the high temporal resolution dataset. This results in lower CBF values for this dataset. Moreover, the inclusion of a gamma dispersion kernel also leads to an increase in aBV values, accompanied by even lower values for the CBF. As expected, almost no macrovascular signal is included in the aBV map for the dataset when vascular crushing is applied. CBF, cerebral blood flow

is assigned to the macrovascular component (low aBV) because vascular signal was apparently successfully crushed (Figure 6). When including a dispersion kernel, some small parts of vessels, especially those located within the border zones, were included in the macrovascular component.

TABLE 2 Mean CBF and aBV values for all volunteers

	aBV (%)		CBF (mL/100 g/min)	
	Without Dispersion	With Gamma Dispersion	Without Dispersion	With Gamma Dispersion
High temporal resolution				
Volunteer 1	1.25	2.56	49.46	39.61
Volunteer 2	1.10	2.09	32.59	27.23
Volunteer 3	2.03	3.51	57.67	45.81
Volunteer 4	1.54	2.72	43.05	34.25
Volunteer 5	1.18	2.66	49.77	40.89
Volunteer 6	1.28	2.58	54.71	43.73
Volunteer 7	1.55	2.58	44.70	35.06
Volunteer 8	1.57	2.57	56.97	45.30
Mean	1.44[*,•]	2.66[*,•]	48.62[*]	38.99[*]
Low temporal resolution				
Volunteer 1	0.49	1.81	49.13	45.24
Volunteer 2	0.38	1.20	33.96	32.05
Volunteer 3	0.82	2.94	57.21	52.38
Volunteer 4	0.68	2.23	47.67	42.80
Volunteer 5	0.70	1.78	46.43	45.01
Volunteer 6	0.51	2.04	55.98	50.48
Volunteer 7	0.93	2.07	47.03	43.68
Volunteer 8	0.57	1.85	56.94	51.29
Mean	0.64[*,•]	1.99[*,•]	49.29	45.37
Synthetic low temporal resolution				
Volunteer 1	0.87	2.50	42.24	37.31
Volunteer 2	0.78	1.91	27.70	26.19
Volunteer 3	1.19	3.24	48.20	42.62
Volunteer 4	0.87	2.30	37.38	33.38
Volunteer 5	0.88	2.65	39.75	37.62
Volunteer 6	0.80	2.41	47.50	41.03
Volunteer 7	1.05	2.39	39.01	33.92
Volunteer 8	0.93	0.93	47.73	41.74
Mean	0.92[*,•]	2.29[*,•]	41.19	36.73
Low temporal resolution with vascular crushing				
Volunteer 1	0.06	0.16	29.24	28.69
Volunteer 2	0.06	0.15	17.02	17.83
Volunteer 3	0.05	0.35	41.24	39.68
Volunteer 4	0.04	0.20	29.32	28.62
Volunteer 5	0.04	0.16	26.69	27.18
Volunteer 6	0.05	0.22	36.35	34.76
Volunteer 7	0.05	0.29	32.04	30.68
Volunteer 8	0.04	0.21	39.04	36.89
Mean	0.05[*]	0.22[*]	31.37	30.54

aBV, arterial blood volume; ASL, arterial spin labeling; CBF, cerebral blood flow.

*Statistical difference between models, multivariate ANOVA, $P < .05$

•Statistical difference between temporal resolutions, multivariate ANOVA, $P < .05$.

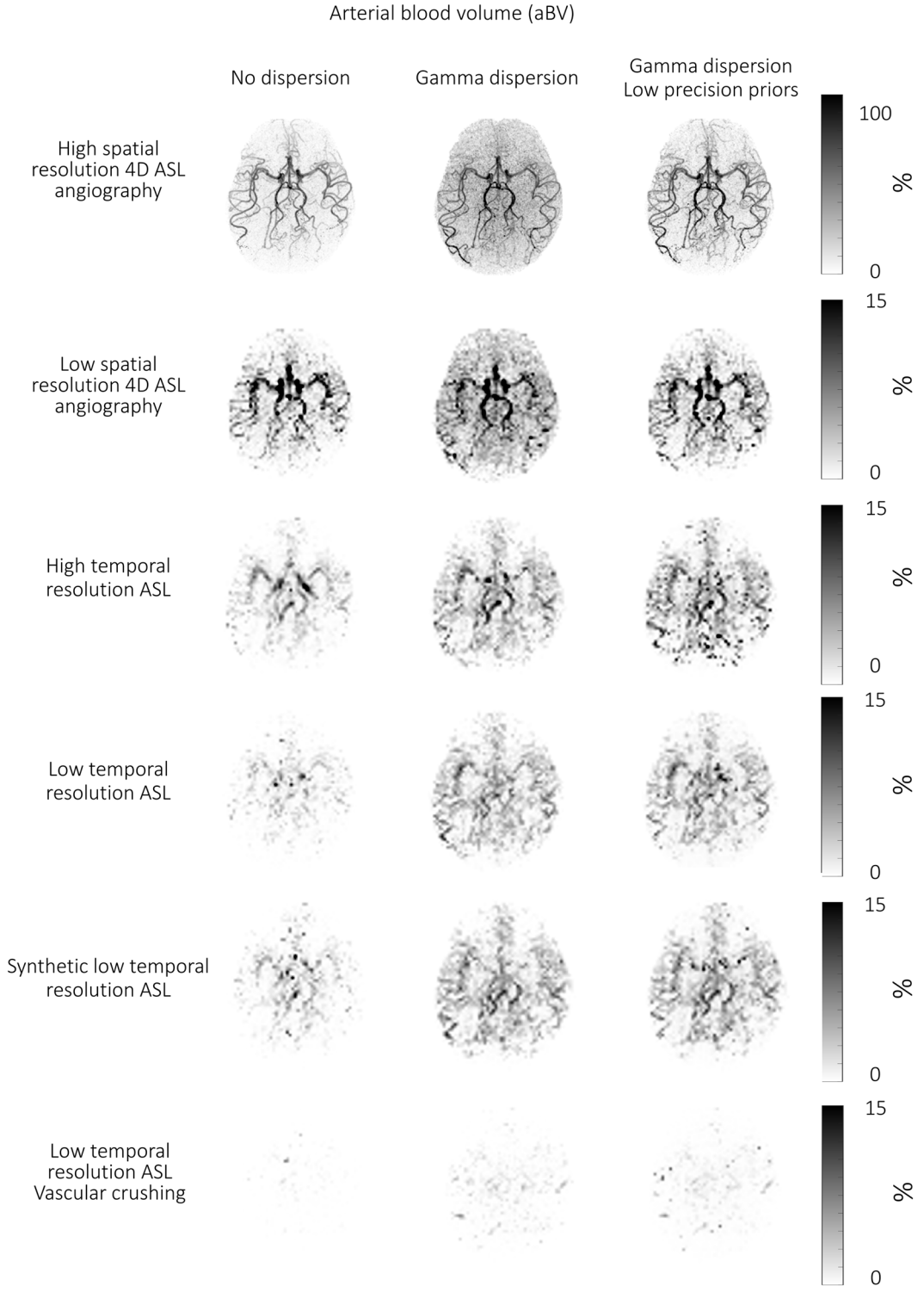

FIGURE 7 ABV maps for the different datasets and different models using the BAT parameter set at 0.55 s. Including a gamma dispersion kernel within the kinetic model leads to an increase of signal intensity for all datasets; in addition, more voxels are fitted, which could indicate that the signal is fitted further down the vascular tree. When the precisions of the gamma dispersion priors were lowered, the model could not fit the signal in all the vessels within the main arteries. The down-sampled 4D ASL angiography, which has the same reconstructed spatial resolution as the high/low temporal resolution datasets, shows higher aBV values compared to the high/low temporal resolution dataset

Using Wilks' statistics, a statistically significant effect was found between the 2 different models that were fitted to the low temporal resolution dataset without ($F(2, 13) = 39{,}807$, $P < .001$; Wilks' $\Lambda = 0.140$) and with ($F(2, 13) = 26.965$, $P < .001$; Wilks' $\Lambda = 0.194$) vascular crushing. However, separate univariate ANOVAs on the outcome

variables revealed significant effects on aBV values ($F(1,14) = 53.478$, $P < .001$ and $F(1, 14) = 45.775$, $P < .001$) for both these datasets but nonsignificant effects on CBF values ($F(1,14) = 1.209$, $P = .290$ and $F(1, 14) = 0.052$, $P = .823$).

The bottom 2 rows of Figure 7 show the aBV maps for the 3 different models for the low temporal resolution datasets with and without vascular crushing. These aBV maps show a decrease of signal for the low temporal resolution dataset compared to the high temporal resolution dataset.

Comparing the aBV and CBF values using a multivariate ANOVA for the different temporal resolutions demonstrated a significant difference between the outcome variables when no dispersion was included in the model ($F(2, 13) = 24.804$, $P < .001$; Wilks' $\Lambda = 0.208$). Separate univariate ANOVAs on the outcome variables revealed a significant effect on the aBV values ($F(1,14) = 41.676$, $P < .001$) and a nonsignificant difference for the CBF values ($F(1,14) = 0.028$, $P = .869$) for the different temporal resolution datasets. The same results were shown between the high and low temporal resolutions when both datasets were fitted with a gamma dispersion kernel included in the model ($F(2, 13) = 18.222$, $P < .001$; Wilks' $\Lambda = 0.263$). Separate univariate ANOVAs showed a significant difference for the aBV values ($F(1,14) = 9.038$, $P = .009$) and a nonsignificant finding for the CBF values ($F(1,14) = 3.889$, $P = .069$)).

The results for the synthetic low temporal resolution ASL dataset demonstrate that similar influences were found when comparing models with and without dispersion kernels, as well as when comparing high versus low temporal resolution (Figures 6 and 7) (Table 2). However, for the synthetic low temporal resolution dataset, the mean aBV values were found to be higher than the mean aBV values of the low temporal resolution dataset (Supporting information Figure S1). As a result, the CBF values of the synthetic low temporal resolution dataset are lower compared to the low temporal resolution dataset.

4 | DISCUSSION

In this study, we investigated the estimation of the macrovascular contribution in multi-timepoint ASL using a 2-component kinetic model. This was studied in 3 different experiments: (1) gold standard data of the macrovascular component was acquired by means of ASL angiography; (2) high temporal resolution ASL-data was analyzed as an optimal multi-timepoint ASL dataset; and (3) more conventional (named *low temporal resolution data* in this paper) temporal resolution data, with and without vascular crushing, was analyzed.

Fitting the 4D-ASL angiography with the model with gamma dispersion (with the standard settings for the priors) showed the best fit and the highest negative FE values; therefore, it is advised to use this macrovascular model when separating macrovascular from tissue signal. A range of initialization values were studied for the BAT parameter. It was shown that the aBV maps were relatively consistent for all initialization values when using the model with the gamma dispersion kernel included. Without including dispersion in the modeling, the maps were much more variable for different BAT initialization values. Because the initialization value of 0.55 s gave the highest negative FE value, this value was used for the rest of the analysis.

Inclusion of a gamma dispersion kernel within the kinetic model led to an increase of aBV values compared to the model without dispersion included, which was consistently shown for all datasets. This was mainly because the arterial signal was fitted much further into the vascular tree; for example, see Figures 3, 6, and 7. This seems logical because dispersion is expected to be more pronounced deeper into the vascular tree, and this is again an argument to include dispersion into the applied model. For the high and low temporal resolution ASL datasets, this increase in aBV values was accompanied by a decrease in CBF values. This is a logical consequence of fitting the macrovascular component deeper into the vascular tree; consequently, one might conclude that inclusion of a gamma dispersion kernel does provide a better estimate of the perfusion signal. This should be confirmed by head-to-head comparison with a gold standard perfusion measurement, such as ^{15}O H_2O positron emission tomography (PET). PET is an accurate and precise method to determine CBF maps and is assumed to be the gold standard for perfusion measurements.[19] It was already shown by Heijtel et al. that ASL CBF measurements are in good agreement with PET CBF estimates; only a small absolute difference was present with main differences in highly vascularized regions.[20] To minimize intermodality differences, a hybrid PET/MRI system would be the optimal option.[21]

The parameters that describe the gamma dispersion kernel are the time to peak (p in seconds) and the sharpness of this kernel (s in seconds^{-1}). The default values of these parameters were based on previous ASL angiography study and implemented for conventional resolution ASL data when the aim is to quantify the ASL signal in perfusion units. To test whether these settings were indeed ideal, it was decided to change the priors of these 2 parameters for the model that fitted the 4D ASL angiography to give them more freedom to see whether a better fit to the data would be achievable. However, the found estimations differed only marginally (see Supporting information Table S1), while showing a large SD. The default settings seem therefore appropriate.

Also studied was whether the temporal resolution of the ASL dataset would influence the separation of macrovascular from perfusion signal. As shown in Figure 6 and Table 2, more signal was present in the aBV map from the high temporal resolution ASL dataset compared to the low-resolution dataset. As the expected consequence, the CBF values were indeed lower for the high temporal resolution data compared to the low temporal resolution data because more signal was included in the aBV map.

Higher temporal resolution ASL datasets, which results in better estimation of the macrovasculature and therefore in higher aBV values, will thus lead to a better separation of the macrovascular and perfusion signal. When a 2-component kinetic model is used, the estimation of the CBF map will thus be more accurate. Temporal resolution of ASL data does, therefore, also influence the separation of the macrovascular and tissue components, which is important when comparing studies and should also be taken into account when designing clinical studies. Woods et al. designed a general framework for the optimal ASL sequence for the estimation of CBF and ATT.[22,23] Zhang et al. examined these different optimized protocols under the effect of dispersion and macrovascular contamination.[24] It was shown that an ASL sequence optimized for both ATT and CBF estimation is also sensitive to macrovascular signal, which makes sense because shorter PLDs are needed to estimate ATT, during which timepoints the labeled blood remains within arteries. This suggests that an ASL sequence optimized for ATT estimations is also suited for the estimation of aBV. This in line with our results (Figures 6 and 7), showing that a higher temporal resolution results in higher aBV values. To further improve the accuracy and precision of the aBV estimation, it is therefore important to sample more densely at shorter PLDs starting from the BAT, that is, the arrival time of the label within the arteries in the imaging volume.

The difference in aBV and CBF values, which are shown in the Supporting information Figure S1, between the original and synthetic low temporal resolution data could probably be attributed to the SNR differences between these 2 datasets originating from the smaller flip angle of the synthetic low temporal resolution dataset. Such a decrease in SNR could have a more profound effect on the perfusion estimate compared to the aBV estimates due to the relatively lower signal of the perfusion component. This might explain the higher aBV and lower CBF values in these synthetic low temporal resolution datasets, but this hypothesis should be proven in future research.

Surprisingly, a large difference was observed between the aBV values obtained from the down-sampled 4D ASL angiography and the high (and low) temporal resolution ASL data. Because the reconstructed spatial resolutions were similar, values that were similar were expected. The aBV data from the ASL angiography data at the same spatial resolution were approximately a factor 10 higher. The aBV values of the ASL data are in line with previous reported values of aBV $< 5\%$ when measured by ASL.[3,25,26] These aBV values in ASL are a combination of macrovascular and microvascular arterial blood volumes and seem to be consistent with cerebral blood volumes measured with PET.[27] However, with PET usually only the microvascular blood volumes are included. Yet, literature values of, for example, the middle cerebral artery diameter do[28] support the larger values, as observed from the down-sampled 4D-ASL angiography data. With a mean diameter of the middle cerebral artery of 3.1 mm and our voxel-size in the X/Y-plane of 3 mm, the volume of the middle cerebral artery within a voxel is around 22 mm^3. Because the total volume of our voxel is 72 mm^3, this results in aBV values up to 30%. Of course, the middle cerebral arter is not traversing straight through a voxel; therefore, the aBV values will be somewhat lower than 30%. However, these values are in good agreement with the observed aBV values for the down-sampled ASL angiography.

The reason for this discrepancy is unknown but might be related to the fact that the dynamic pattern of the macrovascular component is too similar to the perfusion signal for accurate separation or due to differences in vascular crushing between an EPI and a TFE-readout. This last option is supported by the fact that the maximum intensity projection of the macrovascular component in the EPI-data reflects mainly more distal arteries, which are known to exhibit slower blood flow. To rule out that some steps during the postprocessing affected the output of the kinetic model, 2 steps were studied more closely. First, the 4D ASL angiography as well as the downsampled version of this were fitted by only a single component model; that is, only the macrovascular component was included. We further investigated whether the fitting of just this single-component model could have influenced the aBV maps. Figure 8 shows the aBV and CBF maps (A and B) when the 2-component model is fitted to the 4D ASL angiography. The mean values are in agreement with the aBV values (47.06%) for the 1-component fit, and the CBF maps shows mainly noise because almost none of the labeled blood arrived to the tissue for this dataset. This can, therefore, not explain the observed differences in aBV. Secondly, we tested whether downsampling of the aBV map from the high spatial resolution 4D ASL angiographic data would result in similar aBV values as doing the fitting on downsampled multi-PLD data (ie, changing the order of downsampling and fitting; see Figure 8C). Again, similar values were observed (see second row in Figure 7), excluding also this as a possible explanation for the disagreement. Therefore, these results might suggest that aBV values are underestimated in standard ASL datasets due to vascular crushing by the EPI readout. Underestimation of the aBV should thus be expected when interpreting aBV values obtained from multi-PLD EPI data.

Because the voxel size within our study is on the higher end of the range recommended by the ASL white paper in 2015,[29] it is possible that the quantification of our ASL signal was influenced by partial volume effects. During the quantification process, it is possible to correct for these effects, for example by using a local linear regression approach as proposed by Asllani et al.[30] More recently, Chappell et al. proposed a partial volume correction method for multi-timepoint ASL datasets.[31] This method is based on adaptive spatial regularization, partial volume estimates of different tissue types, and differences in kinetics between gray and white matter. However, at this point the macrovasculature is not included as a separate compartment with its own partial volume in the model. Although conceptually not difficult, it does pose some

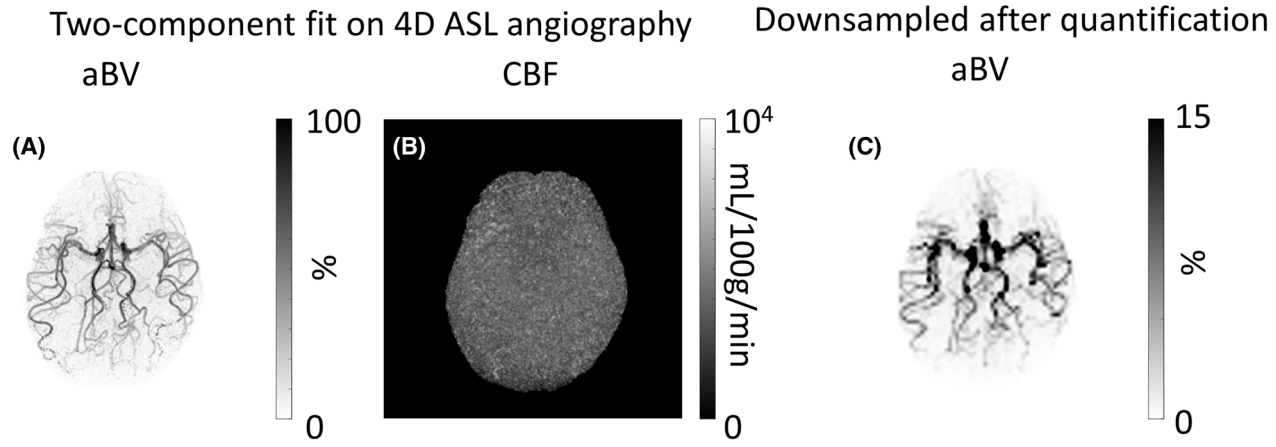

FIGURE 8 aBV and CBF maps (A and B) of volunteer 3 for the 2-component fit to the 4D ASL angiography dataset. This aBV map has similar mean aBV values as obtained with the 1-component fit. The aBV map in C shows the downsampled version of the aBV map as obtained from the high spatial resolution 4D ASL angiography data, which shows comparable aBV values as the aBV map obtained from downsampling the multi-PLD ASL-images, that is, before fitting the model (Figure 7)

challenges since it would require either an estimation of macrovascular fraction from an anatomical scan (as done for gray and white matter, but this is not as easy for the macrovascular component) or the fraction (aBV) should be estimated from the multi-timepoint ASL data. This fraction should then also be taken from one of the tissue fractions, which results in a complicated framework. This would be an important improvement and a necessary step for partial volume correction methods to be applied to the type of data of this study.

5 | CONCLUSION

In this study, the combined estimation of dispersion and macrovascular component was investigated using 4D ASL angiography as a reference for the macrovascular component. It was shown that the model including a gamma dispersion kernel outperformed the other models with respect to the highest mean negative FE and the fitting of the vascular signal further into the vascular tree. The combined estimation of dispersion and macrovascular component subsequently was studied using a high and low temporal resolution ASL dataset. For both datasets, inclusion of a gamma dispersion kernel resulted in a statistically significant increase in aBV values and decreased CBF values. Visual inspection allowed correct identification of arterial signals further down the arterial tree, showing that inclusion of a gamma dispersion kernel within the 2-component kinetic model improves separation of macrovascular from perfusion signal. Compared to the low temporal resolution aBV values, statistically significant higher aBV values were found for the high temporal resolution ASL dataset. This also resulted in lower CBF values for the high temporal resolution ASL dataset; therefore, the separation is also influenced by the temporal resolution of the ASL dataset. Finally, the results suggest that an EPI-readout crushes some vascular signal, resulting in an underestimation of aBV values.

ACKNOWLEDGMENT

This work is part of the research program Innovational Research Incentives Scheme VICI with project number 016.160.351, which is financed by the Netherlands Organisation for Scientific Research (NWO). M.A.C. and M.C. are supported by the Engineering and Physical Sciences Research Council UK (EP/P012361/1).

ORCID

Merlijn C. E. van der Plas https://orcid.org/0000-0003-2240-8405
Sophie Schmid https://orcid.org/0000-0003-0750-7798
Michael A. Chappell https://orcid.org/0000-0003-1802-4214
Matthias J. P. van Osch https://orcid.org/0000-0001-7034-8959

REFERENCES

1. MacIntosh BJ, Lindsay AC, Kylintireas I, et al. Multiple inflow pulsed arterial spin-labeling reveals delays in the arterial arrival time in minor stroke and transient ischemic attack. *AJNR Am J Neuroradiol*. 2010;31:1892-1894.
2. Yoshiura T, Hiwatashi A, Yamashita K, et al. Simultaneous measurement of arterial transit time, arterial blood volume, and cerebral blood flow using arterial spin-labeling in patients with Alzheimer disease. *Am J Neuroradiol*. 2009;30:1388-1393.
3. Chappell MA, MacIntosh BJ, Donahue MJ, et al. Separation of macrovascular signal in multi-inversion time arterial spin labelling MRI. *Magn Reson Med*. 2010;63:1357-1365.
4. Pinto J, Chappell MA, Okell TW, et al. Calibration of arterial spin labeling data-potential pitfalls in post-processing. *Magn Reson Med*. 2020;83:1222-1234.

5. Buxton RB, Uludag K, Dubowitz DJ, Liu TT. Modeling the hemodynamic response to brain activation. *Neuroimage*. 2004;23(suppl 1):S220-S233.
6. Chappell MA, Woolrich MW, Kazan S, et al. Modeling dispersion in arterial spin labeling: validation using dynamic angiographic measurements. *Magn Reson Med*. 2013;69:563-570.
7. Hrabe J, Lewis DP. Two analytical solutions for a model of pulsed arterial spin labeling with randomized blood arrival times. *J Magn Reson*. 2004;167:49-55.
8. Gallichan D, Jezzard P. Modeling the effects of dispersion and pulsatility of blood flow in pulsed arterial spin labeling. *Magn Reson Med*. 2008;60:53-63.
9. Bokkers R, van Laar PJ, van de Ven K, et al. Arterial spin-labeling MR imaging measurements of timing parameters in patients with a carotid artery occlusion. *AJNR Am J Neuroradiol*. 2008;29:1698-1703.
10. Uchino H, Ito M, Fujima N, et al. A novel application of four-dimensional magnetic resonance angiography using an arterial spin labeling technique for noninvasive diagnosis of Moyamoya disease. *Clin Neurol Neurosurg*. 2015;137:105-111.
11. Zhang K, Yun SD, Shah NJ. Tripled readout slices in multi time-point pCASL using multiband look-locker EPI. *PLoS One*. 2015;10:e0141108.
12. Gunther M, Bock M, Schad LR. Arterial spin labeling in combination with a looklocker. *Magn Reson Med*. 2001;46:974-984.
13. Bernstein MA, King KF, Zhou XJ. *Handbook of MRI Pulse Sequences*. Amsterdam, The Netherlands: Elsevier Academic Press; 2004.
14. Jezzard P, Chappell MA, Okell TW. Arterial spin labeling for the measurement of cerebral perfusion and angiography. *J Cereb Blood Flow Metab*. 2017;38:603-626.
15. Chappell MA, Groves AR, Whitcher B, Woolrich MW. Variational Bayesian inference for a nonlinear forward model. *IEEE Trans Signal Process*. 2009;57:223-236.
16. Groves AR, Chappell MA, Woolrich MW. Combined spatial and non-spatial prior for inference on MRI time-series. *Neuroimage*. 2009;45:795-809.
17. Günther M. Highly efficient accelerated acquisition of perfusion inflow series by cycled arterial spin labeling. In Proceedings of the 6th Annual Meeting of the ISMRM, Berlin, Germany, 2007. Abstract 380.
18. van der Plas MCE, Teeuwisse WM, Schmid S, Chappell M, van Osch MJP. High temporal resolution arterial spin labeling MRI with whole-brain coverage by combining time-encoding with Look-Locker and simultaneous multi-slice imaging. *Magn Reson Med*. 2019;81:3734-3744.
19. Fan AP, Jahanian H, Holdsworth SJ, Zaharchuk G. Comparison of cerebral blood flow measurement with [15O]-water positron emission tomography and arterial spin labeling magnetic resonance imaging: a systematic review. *J Cereb Blood Flow Metab*. 2016;36:842-861.
20. Heijtel D, Mutsaerts H, Bakker E, et al. Accuracy and precision of pseudo-continuous arterial spin labeling perfusion during baseline and hypercapnia: a head-to-head comparison with 15O H2O positron emission tomography. *Neuroimage*. 2014;92:182-192.
21. Catana C, Drzezga A, Heiss WD, Rosen BR. PET/MRI for neurologic applications. *J Nucl Med*. 2012;53:1916-1925.
22. Woods JG, Chappell MA, Okell TW. A general framework for optimizing arterial spin labeling MRI experiments. *Magn Reson Med*. 2019;81:2474-2488.
23. Woods JG, Chappell MA, Okell TW. Designing and comparing optimized pseudo-continuous arterial spin labeling protocols for measurement of cerebral blood flow. *Neuroimage*. 2020;223:117246.
24. Zhang LX, Woods JG, Okell TW, Chappell MA. Examination of optimized protocols for pCASL: sensitivity to macrovascular contamination, flow dispersion, and prolonged arterial transit time. *Magn Reson Med*. 2021;86:2208-2219.
25. Petersen ET, Lim T, Golay X. Model-free arterial spin labeling quantification approach for perfusion MRI. *Magn Reson Med*. 2006;55:219-232.
26. An H, Lin W. Cerebral venous and arterial blood volumes can be estimated separately in humans using magnetic resonance imaging. *Magn Reson Med*. 2002;48:583-588.
27. Greenberg J, Alavi A, Reivich M, Kuhl D, Uzzell B. Local cerebral blood volume response to carbon dioxide in man. *Circ Res*. 1978;43:324-331.
28. Rai AT, Hogg JP, Cline B, Hobbs G. Cerebrovascular geometry in the anterior circulation: an analysis of diameter, length and the vessel taper. *J Neurointerv Surg*. 2013;5:371-375.
29. Alsop DC, Detre JA, Golay X, et al. Recommended implementation of arterial spin labeled perfusion MRI for clinical applications: a consensus of the ISMRM perfusion study group and the European Consortium for ASL in Dementia. *Magn Reson Med*. 2015;73:102-116.
30. Asllani I, Borogovac A, Brown TR. Regression algorithm correcting for partial volume effects in arterial spin labeling MRI. *Magn Reson Med*. 2008;60:1362-1371.
31. Chappell MA, Groves AR, MacIntosh BJ, et al. Partial volume correction of multiple inversion time arterial spin labeling MRI data. *Magn Reson Med*. 2011;65:1173-1183.

SUPPORTING INFORMATION

Additional Supporting Information may be found online in the Supporting Information section.

FIGURE S1 Comparison between mean arterial blood volumes and cerebral blood flow values between high, low and synthetic low temporal resolution with and without dispersion kernel included in the kinetic model. Similar influences are shown when comparing the results with and without the inclusion of a dispersion kernel

TABLE S1 Mean values for the two dispersion parameters Log(s) and Log(s*p) for the model with the default precisions for these parameters and the model with more freedom, where the precisions were lowered from 1.0 to 0.1. These values were calculated within an angiographic mask for the 4D ASL angiography datasets. Giving these dispersion parameters more freedom to fit the data resulted in minor changes compared to the default settings

How to cite this article: van der Plas MCE, Craig M, Schmid S, Chappell MA, van Osch MJP. Validation of the estimation of the macrovascular contribution in multi-timepoint arterial spin labeling MRI using a 2-component kinetic model. *Magn Reson Med*. 2022;87:85–101. https://doi.org/10.1002/mrm.28960